

Fourth order summation-by-parts finite difference methods for 3-D elastic wave propagation in curvilinear coordinates with mesh refinement interfaces

Lu Zhang Siyang Wang N. Anders Petersson

January 2, 2020

Abstract

We analyze

1 Introduction

2 The isotropic elastic wave equation

We consider the time dependent isotropic elastic wave equation in three dimensions. The problem is defined on a curvilinear domain $\mathbf{x} \in \Omega$, $\mathbf{x} = (x^1, x^2, x^3)^T$ with a mesh refinement interface Γ . We partition the domain Ω into two subdomains Ω^f and Ω^c such that the interface Γ is aligned with a subdomain boundary with $\Omega = \Omega^f \cup \Omega^c$ and $\Gamma = \Omega^f \cap \Omega^c$. Denote $\mathbf{F} = (F_1, F_2, F_3)^T$ to be the three dimensional displacement vector on Ω^f and $\mathbf{C} = (C_1, C_2, C_3)^T$ to be the three dimensional displacement vector on Ω^c . By introducing smooth one-to-one mapping

$$\mathbf{x}^f = \mathbf{X}^f(\mathbf{r}) : \Omega_r^f = [0, 1]^3 \rightarrow \Omega^f \subset \mathbb{R}^3$$

with $\mathbf{X}^f(\mathbf{r}) = (x^{f,1}(\mathbf{r}), x^{f,2}(\mathbf{r}), x^{f,3}(\mathbf{r}))^T$, $\mathbf{r} = (r^1, r^2, r^3)^T$, $0 \leq r^i \leq 1$, $i = 1, 2, 3$ and one-to-one mapping

$$\mathbf{x}^c = \mathbf{X}^c(\mathbf{r}) : \Omega_r^c = [0, 1]^3 \rightarrow \Omega^c \subset \mathbb{R}^3$$

with $\mathbf{X}^c(\mathbf{r}) = (x^{c,1}(\mathbf{r}), x^{c,2}(\mathbf{r}), x^{c,3}(\mathbf{r}))^T$, $\mathbf{r} = (r^1, r^2, r^3)^T$, $0 \leq r^i \leq 1$, $i = 1, 2, 3$, the elastic wave equation can be written in curvilinear coordinates as

$$\begin{aligned} \rho^f \frac{\partial^2 \mathbf{F}}{\partial^2 t} &= \frac{1}{J^f} \left[\partial_1(A_1^f \nabla \mathbf{F}) + \partial_2(A_2^f \nabla \mathbf{F}) + \partial_3(A_3^f \nabla \mathbf{F}) \right], \quad \mathbf{r} \in \Omega_r^f, \quad t \geq 0, \\ \rho^c \frac{\partial^2 \mathbf{C}}{\partial^2 t} &= \frac{1}{J^c} [\partial_1(A_1^c \nabla \mathbf{C}) + \partial_2(A_2^c \nabla \mathbf{C}) + \partial_3(A_3^c \nabla \mathbf{C})], \quad \mathbf{r} \in \Omega_r^c, \quad t \geq 0, \end{aligned} \quad (1)$$

where ρ^f and ρ^c are density functions for fine domain Ω^f and coarse domain Ω^c respectively, and $\partial_i = \frac{\partial}{\partial r_i}$, $\nabla = (\partial_1, \partial_2, \partial_3)$. For the rest of paper, we introduce a notation $\{\cdot, \cdot\}$ which represents one of variable is used in an equation, then

$$\begin{aligned} A_1^{\{f,c\}} \nabla \{\mathbf{F}, \mathbf{C}\} &:= N_{11}^{\{f,c\}} \partial_1 \{\mathbf{F}, \mathbf{C}\} + N_{12}^{\{f,c\}} \partial_2 \{\mathbf{F}, \mathbf{C}\} + N_{13}^{\{f,c\}} \partial_3 \{\mathbf{F}, \mathbf{C}\}, \\ A_2^{\{f,c\}} \nabla \{\mathbf{F}, \mathbf{C}\} &:= N_{21}^{\{f,c\}} \partial_1 \{\mathbf{F}, \mathbf{C}\} + N_{22}^{\{f,c\}} \partial_2 \{\mathbf{F}, \mathbf{C}\} + N_{23}^{\{f,c\}} \partial_3 \{\mathbf{F}, \mathbf{C}\}, \\ A_3^{\{f,c\}} \nabla \{\mathbf{F}, \mathbf{C}\} &:= N_{31}^{\{f,c\}} \partial_1 \{\mathbf{F}, \mathbf{C}\} + N_{32}^{\{f,c\}} \partial_2 \{\mathbf{F}, \mathbf{C}\} + N_{33}^{\{f,c\}} \partial_3 \{\mathbf{F}, \mathbf{C}\}, \end{aligned}$$

with

$$N_{ij}^{\{f,c\}} = J^{\{f,c\}}(P_i^{\{f,c\}})^T M^{\{f,c\}} P_j^{\{f,c\}}.$$

Here, $M^{\{f,c\}}$ is 6×6 stiffness matrix and it is symmetric and positive definite. Especially, for isotropic elastic wave equation, we have

$$\begin{aligned} M_{11}^{\{f,c\}} &= \begin{pmatrix} 2\mu^{\{f,c\}} + \lambda^{\{f,c\}} & 0 & 0 \\ 0 & \mu^{\{f,c\}} & 0 \\ 0 & 0 & \mu^{\{f,c\}} \end{pmatrix}, \quad M_{12}^{\{f,c\}} = \begin{pmatrix} 0 & \lambda^{\{f,c\}} & 0 \\ \mu^{\{f,c\}} & 0 & 0 \\ 0 & 0 & 0 \end{pmatrix}, \\ M_{22}^{\{f,c\}} &= \begin{pmatrix} \mu^{\{f,c\}} & 0 & 0 \\ 0 & 2\mu^{\{f,c\}} + \lambda^{\{f,c\}} & 0 \\ 0 & 0 & \mu^{\{f,c\}} \end{pmatrix}, \quad M_{13}^{\{f,c\}} = \begin{pmatrix} 0 & 0 & \lambda^{\{f,c\}} \\ 0 & 0 & 0 \\ \mu^{\{f,c\}} & 0 & 0 \end{pmatrix}, \\ M_{33}^{\{f,c\}} &= \begin{pmatrix} \mu^{\{f,c\}} & 0 & \lambda^{\{f,c\}} \\ 0 & \mu^{\{f,c\}} & 0 \\ 0 & 0 & 2\mu^{\{f,c\}} + \lambda^{\{f,c\}} \end{pmatrix}, \quad M_{23}^{\{f,c\}} = \begin{pmatrix} 0 & 0 & 0 \\ 0 & 0 & \lambda^{\{f,c\}} \\ 0 & \mu^{\{f,c\}} & 0 \end{pmatrix}, \\ M_{31}^{\{f,c\}} &= (M_{13}^{\{f,c\}})^T, \quad M_{32}^{\{f,c\}} = (M_{23}^{\{f,c\}})^T, \quad M_{21}^{\{f,c\}} = (M_{12}^{\{f,c\}})^T. \end{aligned}$$

Here, $\lambda^{\{f,c\}}$ and $\mu^{\{f,c\}}$ are the first and second Láme parameters respectively, which are determined by the properties of the materials. We refer to Appendix A for the definitions of matrices $P_i^{\{f,c\}}$, $i = 1, 2, 3$. For the matrices $N_{ij}^{\{f,c\}}$, we have that $N_{ii}^{\{f,c\}}$ are symmetric positive definite, and $N_{ij}^{\{f,c\}} = (N_{ji}^{\{f,c\}})^T$, $i, j = 1, 2, 3$. The Jacobian of transformation is $J^{\{f,c\}} = \det(\mathbf{a}_1^{\{f,c\}}, \mathbf{a}_2^{\{f,c\}}, \mathbf{a}_3^{\{f,c\}})$, $0 < J^{\{f,c\}} < \infty$, with the derivative of the forward mapping,

$$\mathbf{a}_k^{\{f,c\}} := \partial_k \mathbf{x}^{\{f,c\}} = \left(\frac{\partial x^{\{f,c\},1}}{\partial r^k}, \frac{\partial x^{\{f,c\},2}}{\partial r^k}, \frac{\partial x^{\{f,c\},3}}{\partial r^k} \right)^T, \quad k = 1, 2, 3,$$

and the backward mapping,

$$\mathbf{a}^{\{f,c\},k} := \nabla^{\{f,c\}} r^k = \left(\frac{\partial r^k}{\partial x^{\{f,c\},1}}, \frac{\partial r^k}{\partial x^{\{f,c\},2}}, \frac{\partial r^k}{\partial x^{\{f,c\},3}} \right)^T := (\xi_{1k}^{\{f,c\}}, \xi_{2k}^{\{f,c\}}, \xi_{3k}^{\{f,c\}})^T, \quad k = 1, 2, 3.$$

The metric relation is given by [5],

$$\mathbf{a}^{\{f,c\},i} = \frac{1}{J^{\{f,c\}}} (\mathbf{a}_j^{\{f,c\}} \times \mathbf{a}_k^{\{f,c\}}), \quad (i, j, k) \text{ cycle.}$$

Denote the unit outward normal $\mathbf{n}_i^{\{f,c\},\pm} = (n_i^{\{f,c\},\pm,1}, n_i^{\{f,c\},\pm,2}, n_i^{\{f,c\},\pm,3})^T$, $i = 1, 2, 3$, for the boundaries of i 'th direction on subdomain $\Omega^{\{f,c\}}$, then

$$\begin{aligned} \mathbf{n}_i^{\{f,c\},\pm} &:= (n_i^{\{f,c\},\pm,1}, n_i^{\{f,c\},\pm,2}, n_i^{\{f,c\},\pm,3})^T = \pm \frac{\nabla^{\{f,c\}} r^i}{|\nabla^{\{f,c\}} r^i|} \\ &= \pm \frac{(\xi_{1i}^{\{f,c\}}, \xi_{2i}^{\{f,c\}}, \xi_{3i}^{\{f,c\}})^T}{\sqrt{(\xi_{1i}^{\{f,c\}})^2 + (\xi_{2i}^{\{f,c\}})^2 + (\xi_{3i}^{\{f,c\}})^2}}, \end{aligned}$$

here, '+' corresponds to $r^{\{f,c\},i} = 1$ and '-' corresponds to $r^{\{f,c\},i} = 0$. At the interface $r^{f,3} = 0$ ($r^{c,3} = 1$), the traction vectors and displacement vectors are continuous with

$$\frac{A_3^f \nabla \mathbf{F}}{J^f |\nabla^f r^3|} = \frac{A_3^c \nabla \mathbf{C}}{J^c |\nabla^c r^3|}, \quad \mathbf{F} = \mathbf{C}. \quad (2)$$

By ignoring boundaries in $r^{\{f,c\},1}$, $r^{\{f,c\},2}$ directions and boundaries as $r^{c,3} \rightarrow 0$, $r^{f,3} \rightarrow 1$, then we can prove the problem is well-posed with a similar analysis as in [1, 3].

3 The spatial discretization

In this section, we describe the spatial discretization for the problem (1). We firstly introduce the SBP operator for the first and second spatial derivative with scalar variable in one dimension and then extend the SBP operators to vector variables in three dimensions.

3.1 SBP operators in 1D

Consider a uniform discretization of the domain $x \in [0, 1]$ with the grids,

$$\tilde{\mathbf{x}} = [x_0, x_1, \dots, x_n, x_{n+1}]^T, \quad x_i = (i-1)h, \quad i = 0, 1, \dots, n, n+1, \quad h = 1/(n-1),$$

where $i = 1, n$ correspond to the grid points on the boundary, and $i = 0, n+1$ are ghost points outside of the physical domain. The operator $D \approx \frac{\partial}{\partial x}$ is a first derivative SBP operator if

$$(\mathbf{u}, D\mathbf{v})_h = -(D\mathbf{u}, \mathbf{v})_h - u_1 v_1 + u_n v_n, \quad (3)$$

with a scalar product

$$(\mathbf{u}, \mathbf{v})_h = h \sum_{i=1}^n \omega_i u_i v_i. \quad (4)$$

Here, $0 < \omega_i < \infty$ are the weights of scalar product. The SBP operator D has a centered difference stencil at the grid points away from the boundary and the corresponding weights $\omega_i = 1$. To satisfy the SBP identity (3), the coefficients in D are modified at a few points near the boundary and the corresponding weights $\omega_i \neq 1$. The operator D does not use any ghost points.

To discretize the elastic wave equation, we also need to approximate the second derivative with variable coefficient $(\gamma(x)u_x)_x$. Here, the known function $\gamma(x) > 0$ describes the property of the material. There are two different fourth order accurate SBP operators for the approximation of $(\gamma(x)u_x)_x$. The first one $\tilde{G}(\gamma)\mathbf{u} \approx (\gamma(x)u_x)_x$, derived by Sjögren and Petersson [4], uses one ghost point outside each boundary, and satisfies the second derivative SBP identity,

$$(\mathbf{u}, \tilde{G}(\gamma)\mathbf{v})_h = -P_\gamma(\mathbf{u}, \mathbf{v}) - u_1 \gamma_1 \tilde{\mathbf{b}}_1 \mathbf{v} + u_n \gamma_n \tilde{\mathbf{b}}_n \mathbf{v}. \quad (5)$$

Here, the bilinear form $P_\gamma(\cdot, \cdot)$ is symmetric and positive semi-definite, and does not use any ghost points. The operators $\tilde{\mathbf{b}}_1$ and $\tilde{\mathbf{b}}_n$ approximate the first derivative on the left and right boundaries, respectively. Using the left boundary as an example, we have

$$\tilde{\mathbf{b}}_1 \mathbf{v} = \frac{1}{h} \sum_{i=0}^4 d_i v_i, \quad (6)$$

as the fourth order accurate approximation of $u_x(x_1)$. We note that the notation $\tilde{G}(\gamma)\mathbf{v}$ implies that the operator \tilde{G} uses \mathbf{v} on all grid points $\tilde{\mathbf{x}}$, but $\tilde{G}(\gamma)\mathbf{v}$ only returns values on the grid \mathbf{x} without ghost points. Therefore, when writing in matrix form, \tilde{G} is a non-square matrix of size n by $n+2$.

The other SBP operator $G(\gamma)\mathbf{u} \approx (\gamma(u_x)_x)_x$ is developed by Mattsson [2] without using any ghost points, and satisfies a similar SBP identity,

$$(\mathbf{u}, G(\gamma)\mathbf{v})_h = -P_\gamma(\mathbf{u}, \mathbf{v}) - u_1\gamma_1\mathbf{b}_1\mathbf{v} + u_n\gamma_n\mathbf{b}_n\mathbf{v}. \quad (7)$$

Here, \mathbf{b}_1 and \mathbf{b}_n are also finite difference operators for the first derivative at the boundaries, but are constructed to third order accurate,

$$\mathbf{b}_1\mathbf{v} = \frac{1}{h} \sum_{i=1}^4 d_i v_i. \quad (8)$$

In this case, $G(\gamma)$ is square in matrix form.

For the second derivative SBP operators $\tilde{G}(\gamma)$ and $G(\gamma)$, both of them use a fourth order five points centered difference stencil to approximate $(\gamma u_x)_x$ on the interior points away from the boundaries. For the first and the last six grid points close to the boundaries, the operators $G(\gamma)$ and $\tilde{G}(\gamma)$ use second order accurate one-sided difference stencils. They are designed to satisfy (7) and (5), respectively. In the following sections, we use both of them to develop a multi-block finite difference discretization for the elastic wave equation.

3.2 Semi-discretization of the elastic wave equation

In this section, we discretize the elastic wave equation (1) with mesh refinement interface Γ . The ratio of the mesh size for subdomains Ω_r^f and Ω_r^c is $1 : 2$, that is we assume uniform mesh size h for Ω_r^f and $2h$ for Ω_r^c with $h(n^h - 1) = 1$ and $2h(n^{2h} - 1) = 1$, other ratios can be treated analogously. Figure 1 gives an illustration of the discretization of a physical domain. We focus on the numerical

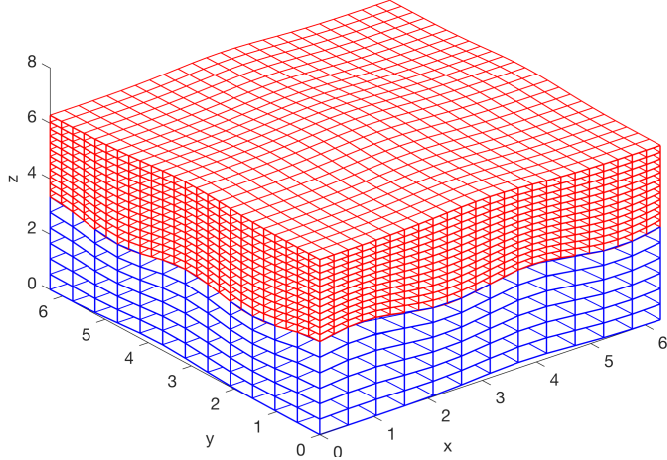


Figure 1: The sketch for the spatial discretization of physical domain Ω . The blue region is the spacial discretization of coarse subdomain Ω^c and the red region is the spatial discretization of fine domain Ω^f .

treatment of the interface conditions (2) and suppose boundaries are periodic in directions 1 and 2, ignore the boundaries in direction 3. In Figure 2, we fix $y = 0$ and present the x - z section of the domain Ω . To condense notations, we introduce the multi-index notations

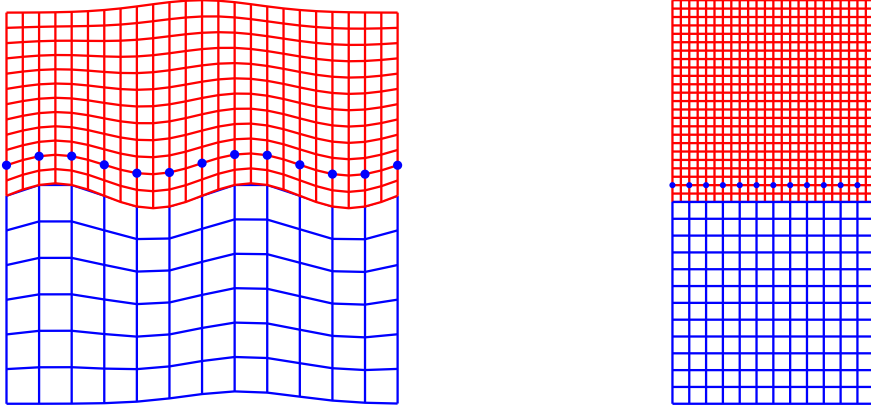


Figure 2: The sketch of spacial discretization of x - z section with $y = 0$. From the left to the right are for physcail domain and parameter space respectively. The blue dots are the ghost points for coarse domain Ω^c .

$$\mathbf{i} = (i, j, k), \quad \mathbf{r}_i = (r_i^1, r_j^2, r_k^3), \quad \mathbf{x}_i^{\{f,c\}} = (x_i^{\{f,c\},1}, x_j^{\{f,c\},2}, x_k^{\{f,c\},3}), \quad \mathbf{x}_i^{\{f,c\}} = \mathbf{X}^{\{f,c\}}(\mathbf{r}_i).$$

Note that for $\mathbf{x}_i^f \in \Omega^f$, we have $i \in [1, n^h]$, $j \in [1, n^h]$, $k \in [1, n^h]$; for $\mathbf{x}_i^c \in \Omega^c$, we have $i \in [1, n^{2h}]$, $j \in [1, n^{2h}]$, $k \in [1, n^{2h}]$; for $\mathbf{x}_i^c \in \Gamma \cap \Omega^c := \Gamma^c$, we have $i \in [1, n^{2h}]$, $j \in [1, n^{2h}]$, $k = n^{2h}$; for $\mathbf{x}_i^f \in \Gamma \cap \Omega^f := \Gamma^f$, we have $i \in [1, n^h]$, $j \in [1, n^h]$, $k = 1$; for $\mathbf{x}_i^f \in \Omega^f \setminus \Gamma := \overline{\Gamma^f}$, we have $i \in [1, n^h]$, $j \in [1, n^h]$, $k \in [2, n^h]$. Now, denote the grid functions in Ω^f and Ω^c as

$$\mathbf{f} = (\mathbf{f}^1, \mathbf{f}^2, \mathbf{f}^3)^T \quad \text{and} \quad \mathbf{c} = (\mathbf{c}^1, \mathbf{c}^2, \mathbf{c}^3)^T$$

respectively. Here,

$$\mathbf{f}^l \approx F_l(\mathbf{r}), \quad \mathbf{X}^f(\mathbf{r}) \in \Omega^f, \quad l = 1, 2, 3,$$

and

$$\mathbf{c}^l \approx C_l(\mathbf{r}), \quad \mathbf{X}^c(\mathbf{r}) \in \Omega^c \quad l = 1, 2, 3.$$

Furthermore, we define \mathbf{f}_Γ as the grid function for $\mathbf{X}^f(\mathbf{r}) \in \Gamma^f$, \mathbf{c}_Γ to be the grid function for $\mathbf{X}^c(\mathbf{r}) \in \Gamma^c$ and $\mathbf{f}_{\overline{\Gamma}}$ as the grid function for $\mathbf{X}^f(\mathbf{r}) \in \overline{\Gamma^f}$. Particularly, we define $\tilde{\mathbf{c}} = (\tilde{\mathbf{c}}^1, \tilde{\mathbf{c}}^2, \tilde{\mathbf{c}}^3)^T$ as the grid function which contain both grids in Ω^c and ghost points outside of Ω^c with $i \in [1, n^{2h}]$, $j \in [1, n^{2h}]$, $k \in [0, n^{2h} + 1]$. Then we approximate the elastic wave equation (1) on Ω^c by

$$\varrho^{2h} \mathbf{c}_{tt} = (\mathcal{J}^{2h})^{-1} \left(\sum_{l=1}^2 \mathcal{G}_l^{2h}(N_{ll}) \mathbf{c} + \tilde{\mathcal{G}}_3^{2h}(N_{33}) \tilde{\mathbf{c}} + \sum_{l=1}^3 \sum_{m=1, m \neq l}^3 \mathcal{D}_l^{2h}(\mathcal{N}_{lm}^{2h} \mathcal{D}_m^{2h} \mathbf{c}) \right) := \tilde{L}^{2h} \tilde{\mathbf{c}}, \quad (9)$$

where

$$\varrho^{2h} = \begin{pmatrix} \boldsymbol{\rho}^{2h} & & \\ & \boldsymbol{\rho}^{2h} & \\ & & \boldsymbol{\rho}^{2h} \end{pmatrix}, \quad \mathcal{J}^{2h} = \begin{pmatrix} \mathbf{J}^{2h} & & \\ & \mathbf{J}^{2h} & \\ & & \mathbf{J}^{2h} \end{pmatrix} \quad (10)$$

with both $\boldsymbol{\rho}^{2h}$ and \mathbf{J}^{2h} are $n^{2h} n^{2h} n^{2h} \times n^{2h} n^{2h} n^{2h}$ diagonal matrix with diagonal entries are values of density function ρ^c and Jacobian of transformation J^c on the grids in Ω^c respectively. And $\mathcal{G}_l^{2h}(N_{ll})$, $l = 1, 2$ are defined as

$$\mathcal{G}_l^{2h}(N_{ll}) = \begin{pmatrix} G_l^{2h}(N_{ll}^{11}) & G_l^{2h}(N_{ll}^{12}) & G_l^{2h}(N_{ll}^{13}) \\ G_l^{2h}(N_{ll}^{21}) & G_l^{2h}(N_{ll}^{22}) & G_l^{2h}(N_{ll}^{23}) \\ G_l^{2h}(N_{ll}^{31}) & G_l^{2h}(N_{ll}^{32}) & G_l^{2h}(N_{ll}^{33}) \end{pmatrix}, \quad (11)$$

with $G_l^{2h}(N_{ll}^{ij})$, $i, j = 1, 2, 3$, are $n^{2h}n^{2h}n^{2h} \times n^{2h}n^{2h}n^{2h}$ matrix which is from the central difference operator for second derivative with variable coefficient in direction l , the superscript ij represents the i 'th row and j 'th column of matrix N_{ll} . As for $\tilde{\mathcal{G}}_3^{2h}(N_{33})$, it has a structure

$$\tilde{\mathcal{G}}_3^{2h}(N_{33}) = \begin{pmatrix} \tilde{G}_3^{2h}(N_{33}^{11}) & \tilde{G}_3^{2h}(N_{33}^{12}) & \tilde{G}_3^{2h}(N_{33}^{13}) \\ \tilde{G}_3^{2h}(N_{33}^{21}) & \tilde{G}_3^{2h}(N_{33}^{22}) & \tilde{G}_3^{2h}(N_{33}^{23}) \\ \tilde{G}_3^{2h}(N_{33}^{31}) & \tilde{G}_3^{2h}(N_{33}^{32}) & \tilde{G}_3^{2h}(N_{33}^{33}) \end{pmatrix},$$

where $\tilde{G}_3^{2h}(N_{33}^{ij})$, $i, j = 1, 2, 3$, are $n^{2h}n^{2h}n^{2h} \times n^{2h}n^{2h}(n^{2h} + 2)$ matrices which are defined as in (5) for direction 3. Finally, let's look at the term $\mathcal{D}_l^{2h}(\mathcal{N}_{lm}^{2h}\mathcal{D}_m^{2h})$, $l = 1, 2, 3, m = 1, 2, 3, l \neq m$, we use $\mathcal{D}_1^{2h}(\mathcal{N}_{12}^{2h}\mathcal{D}_2^{2h})$ as an example and other cases are analogous,

$$\mathcal{D}_1^{2h} = \mathbf{I} \otimes D_1^{2h} \otimes \mathbf{I}_2 \otimes \mathbf{I}_3, \quad \mathcal{D}_2^{2h} = \mathbf{I} \otimes \mathbf{I}_1 \otimes D_2^{2h} \otimes \mathbf{I}_3,$$

where \mathbf{I} is 3×3 identity matrix, \mathbf{I}_l , $l = 1, 2, 3$ are $n^{2h} \times n^{2h}$ identity matrices, D_1^{2h} is a $n^{2h} \times n^{2h}$ matrix defined in (3) for direction 1 and D_2^{2h} is a matrix of size $n^{2h} \times n^{2h}$ defined in (3) for direction 2. \mathcal{N}_{lm}^{2h} is a 3×3 block matrix with each block to be a $n^{2h}n^{2h}n^{2h} \times n^{2h}n^{2h}n^{2h}$ matrix

$$\mathcal{N}_{lm}^{2h} = \begin{pmatrix} N_{lm}^{11}(\mathbf{r}) & N_{lm}^{12}(\mathbf{r}) & N_{lm}^{13}(\mathbf{r}) \\ N_{lm}^{21}(\mathbf{r}) & N_{lm}^{22}(\mathbf{r}) & N_{lm}^{23}(\mathbf{r}) \\ N_{lm}^{31}(\mathbf{r}) & N_{lm}^{32}(\mathbf{r}) & N_{lm}^{33}(\mathbf{r}) \end{pmatrix}, \quad l = 1, 2, 3, m = 1, 2, 3, l \neq m. \quad (12)$$

Next, we approximate the elastic wave equation (1) on $\overline{\Gamma^f}$

$$\varrho_{\overline{\Gamma}}^h(\mathbf{f}_{\overline{\Gamma}})_{tt} = (\mathcal{J}_{\overline{\Gamma}}^h)^{-1} \left(\sum_{l=1}^3 \left(\mathcal{G}_l^h(N_{ll})\mathbf{f} \Big|_{\overline{\Gamma}} + \sum_{m=1, m \neq l}^3 \mathcal{D}_l^h(\mathcal{N}_{lm}^h \mathcal{D}_m^h \mathbf{f}) \Big|_{\overline{\Gamma}} \right) \right) := L^h \mathbf{f} \Big|_{\overline{\Gamma}}, \quad (13)$$

where $\varrho_{\overline{\Gamma}}^h$ and $\mathcal{J}_{\overline{\Gamma}}^h$ are $3n^h n^h (n^h - 1) \times 3n^h n^h (n^h - 1)$ diagonal matrix, which has a similar definition as in (10), but corresponds to the grids in $\overline{\Gamma^f}$. Lastly, we approximate the elastic wave equation (1) on Γ^f by

$$\varrho_{\Gamma}^h(\mathbf{f}_{\Gamma})_{tt} = (\mathcal{J}_{\Gamma}^h)^{-1} \left(\sum_{l=1}^3 \left(\mathcal{G}_l^h(N_{ll})\mathbf{f} \Big|_{\Gamma} + \sum_{m=1, m \neq l}^3 \mathcal{D}_l^h(\mathcal{N}_{lm}^h \mathcal{D}_m^h \mathbf{f}) \Big|_{\Gamma} \right) \right) + \boldsymbol{\eta} := L^h \mathbf{f} \Big|_{\Gamma} + \boldsymbol{\eta}, \quad (14)$$

with

$$\boldsymbol{\eta} = \varrho_{\Gamma}^h \tilde{\mathcal{P}} \left((\varrho^{2h})^{-1} \tilde{L}^{2h} \tilde{\mathbf{c}} \Big|_{\Gamma} \right) - L^h \mathbf{f} \Big|_{\Gamma}, \quad (15)$$

here, ϱ_{Γ}^h and \mathcal{J}_{Γ}^h are $3n^h n^h \times 3n^h n^h$ diagonal matrix with a similar definition as in (10) with grids on Γ^f . $(\varrho^{2h})^{-1} \tilde{L}^{2h} \tilde{\mathbf{c}} \Big|_{\Gamma}$ is a column vector of size $3n^{2h}n^{2h}$ and its value corresponds to the grids on Γ^c . Moreover, the terms $\mathcal{G}_l^h(N_{ll})$, $l = 1, 2$ and $\mathcal{D}_l^h(\mathcal{N}_{lm}^h \mathcal{D}_m^h)$, $l = 1, 2, 3, m = 1, 2, 3, l \neq m$ in (13)–(14) has similar definitions as in (11)–(12), and $\mathcal{G}_3^h(N_{33})$ is defined by

$$\mathcal{G}_3^h(N_{33}) = \begin{pmatrix} G_3^{2h}(N_{33}^{11}) & G_3^{2h}(N_{33}^{12}) & G_3^{2h}(N_{33}^{13}) \\ G_3^{2h}(N_{33}^{21}) & G_3^{2h}(N_{33}^{22}) & G_3^{2h}(N_{33}^{23}) \\ G_3^{2h}(N_{33}^{31}) & G_3^{2h}(N_{33}^{32}) & G_3^{2h}(N_{33}^{33}) \end{pmatrix},$$

where $G_3^h(N_{33}^{ij}(\mathbf{r}))$, $i, j = 1, 2, 3$, are $n^h n^h n^h \times n^h n^h n^h$ matrix which are defined as in (7) for direction 3. For the simplicity of analysis, we introduce a general notation for the schemes (13) and (14) in

the fine domain Ω^f ,

$$\varrho^h \mathbf{f}_{tt} = \hat{L}^h \mathbf{f} = \begin{cases} L^h \mathbf{f}|_{\Gamma} + \boldsymbol{\eta}, \\ L^h \mathbf{f}|_{\bar{\Gamma}}. \end{cases} \quad (16)$$

The following we are going to look at the interpolation operator \mathbf{P} and restriction operator \mathbf{R} in two dimensions. The stencils for the interpolation operator \mathbf{P} can be easily computed by a Taylor series expansion. In our case, we have the ratio of the mesh size for subdomain Ω^f and Ω^c is $1 : 2$, then if \mathbf{P} is a fourth order interpolation operator in two dimensions, the stencils of \mathbf{P} are illustrated in Figure 3, the stencils for the corresponding restriction operator in two dimensions can be determined by the compatibility between interpolation and restriction operators, $\mathbf{P} = 4\mathbf{R}^T$, and its stencil is presented in Figure 4.

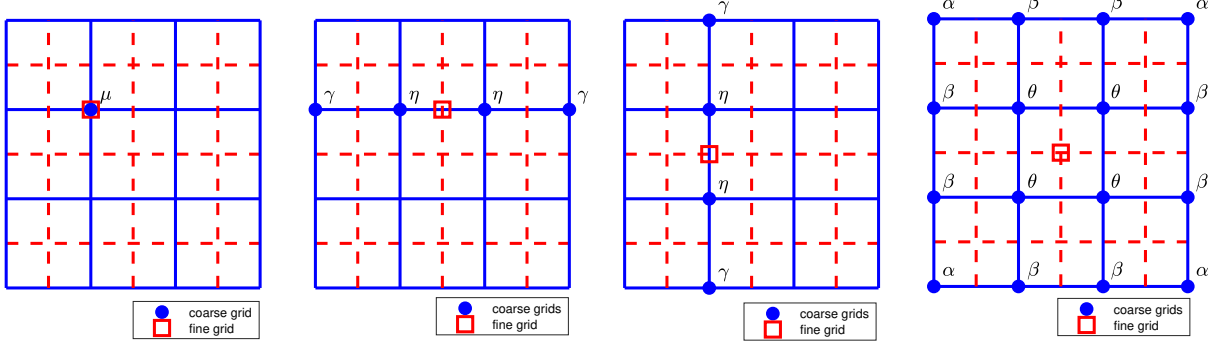


Figure 3: The sketch for the stencils of 4th order interpolation operator \mathcal{P} in two dimensions with parameters $\gamma = -\frac{1}{16}$, $\eta = \frac{9}{16}$, $\mu = 1$, $\alpha = \frac{1}{256}$, $\beta = -\frac{9}{256}$ and $\theta = \frac{81}{256}$.

To proceed the interface conditions, we firstly introduce scaled interpolation and restriction operators

$$\tilde{\mathcal{P}} = (\mathcal{J}_\Gamma^h |\nabla^f r^3|)^{-\frac{1}{2}} \mathcal{P} (\mathcal{J}_\Gamma^{2h} |\nabla^c r^3|)^{\frac{1}{2}}, \quad \tilde{\mathcal{R}} = (\mathcal{J}_\Gamma^{2h} |\nabla^c r^3|)^{-\frac{1}{2}} \mathcal{R} (\mathcal{J}_\Gamma^h |\nabla^f r^3|)^{\frac{1}{2}}.$$

Here, \mathcal{P} is a $3n^{2h}n^{2h}n^{2h} \times 3n^{2h}n^{2h}n^{2h}$ matrix and \mathcal{R} is a $3n^h n^h n^h \times 3n^h n^h n^h$ matrix as

$$\mathcal{P} = \begin{pmatrix} \mathbf{P} & & \\ & \mathbf{P} & \\ & & \mathbf{P} \end{pmatrix}, \quad \mathcal{R} = \begin{pmatrix} \mathbf{R} & & \\ & \mathbf{R} & \\ & & \mathbf{R} \end{pmatrix}, \quad (17)$$

\mathbf{P} is a $n^{2h}n^{2h}n^{2h} \times n^{2h}n^{2h}n^{2h}$ matrix which has stencils as in Figure 3 and \mathbf{R} is a $n^h n^h n^h \times n^h n^h n^h$ matrix has a stencil as in Figure 4. Now, we are ready to state the continuous interface conditions (2), the grid functions \mathbf{f} and \mathbf{c} are coupled through interface conditions,

$$\mathbf{f}|_{\Gamma} = \tilde{\mathcal{P}}(\mathbf{c}|_{\Gamma}), \quad (18)$$

which imposes the continuity of the solution at the interface Γ and

$$|\nabla^c r^3|^{-1} (\mathcal{J}_\Gamma^{2h})^{-1} \tilde{\mathcal{A}}_3^{2h} \tilde{\mathbf{c}}|_{\Gamma} = \tilde{\mathcal{R}} \left(|\nabla^f r^3|^{-1} (\mathcal{J}_\Gamma^h)^{-1} (\mathcal{A}_3^h \mathbf{f}|_{\Gamma} - h\omega_1 \mathcal{J}^h \boldsymbol{\eta}) \right) \quad (19)$$

where we have used the notations

$$\mathcal{A}_3^h \mathbf{f}|_{\Gamma} = \mathcal{N}_{31}^h \mathcal{D}_1^h \mathbf{f}|_{\Gamma} + \mathcal{N}_{32}^h \mathcal{D}_2^h \mathbf{f}|_{\Gamma} + \mathcal{N}_{33}^h \mathcal{D}_3^h \mathbf{f}|_{\Gamma}, \quad (20)$$

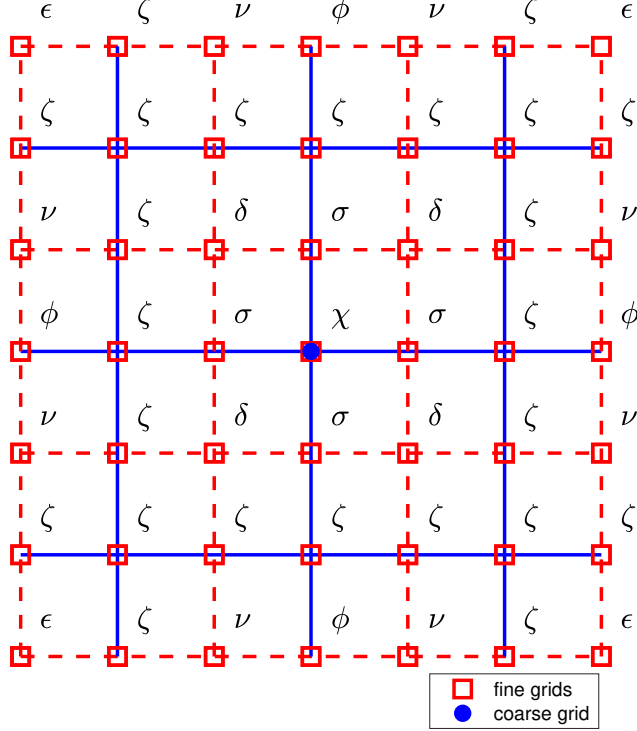


Figure 4: The sketch for the stencil of 4th order restriction operator \mathcal{R} in two dimensions with parameters $\epsilon = \frac{1}{1024}$, $\nu = -\frac{9}{1024}$, $\phi = -\frac{16}{1024}$, $\delta = \frac{81}{1024}$, $\sigma = \frac{144}{1024}$, $\chi = \frac{256}{1024}$ and $\zeta = 0$.

and

$$\tilde{\mathcal{A}}_3^{2h} \tilde{\mathbf{c}}|_{\Gamma} = \mathcal{N}_{31}^{2h} \mathcal{D}_1^{2h} \mathbf{c}|_{\Gamma} + \mathcal{N}_{32}^{2h} \mathcal{D}_2^{2h} \mathbf{c}|_{\Gamma} + \mathcal{N}_{33}^{2h} \tilde{\mathcal{D}}_3^{2h} \tilde{\mathbf{c}}|_{\Gamma}, \quad (21)$$

which imposes the continuity of traction at the interface Γ , here, ω_1 is the first entry in the scalar product (4), and $\tilde{\mathcal{D}}_3^{2h}$ is defined as

$$\tilde{\mathcal{D}}_3^{2h} = \mathbf{I} \otimes \mathbf{I}_1 \otimes \mathbf{I}_2 \otimes \tilde{D}_3^{2h}$$

where \mathbf{I} is 3×3 identity matrix, \mathbf{I}_l , $l = 1, 2$ are $n^{2h} \times n^{2h}$ identity matrices, \tilde{D}_3^{2h} is a $n^{2h} \times (n^{2h} + 2)$ matrix defined in (3) for direction 3.

3.3 Energy estimate

In this section, we investigate the energy estimate for the semi-discrete forms (9) and (16) in section 3.2. Provided periodic boundary condition in directions 1, 2. Let \mathbf{u}, \mathbf{v} be grid functions in Ω^c . We define the three dimensional scalar product in Ω^c

$$(\mathbf{u}, \mathbf{v})_{2h} = 8h^3 \sum_{i=1}^{n^{2h}} \sum_{j=1}^{n^{2h}} \sum_{k=1}^{n^{2h}} \omega_k J_{ijk}^{2h} u_{ijk} v_{ijk}, \quad (22)$$

where J_{ijk}^{2h} located at the $((k-1)n^{2h}n^{2h} + (j-1)n^{2h} + i)$ 'th row and $((k-1)n^{2h}n^{2h} + (j-1)n^{2h} + i)$ 'th column of \mathbf{J}^{2h} , u_{ijk} and v_{ijk} located at the $((k-1)n^{2h}n^{2h} + (j-1)n^{2h} + i)$ 'th row of \mathbf{u}, \mathbf{v} respectively.

The two dimensional scalar product for grid functions on the interface Γ^c

$$\langle \mathbf{u}_{\Gamma^c}, \mathbf{v}_{\Gamma^c} \rangle_{2h} = 4h^2 \sum_{i=1}^{n^{2h}} \sum_{j=1}^{n^{2h}} J_{\Gamma,ij}^{2h} |\nabla^c r^3|_{ij} u_{ij} v_{ij}. \quad (23)$$

with $J_{\Gamma,ij}^{2h}$ located at the $((j-1)n^{2h} + i)$ 'th row and $((j-1)n^{2h} + i)$ 'th column of diagonal matrix \mathbf{J}_{Γ}^{2h} , u_{ij} , v_{ij} are the $((j-1)n^{2h} + i)$ 'th element of u_{Γ^c} and v_{Γ^f} respectively. On the other hand, let \mathbf{u}, \mathbf{v} be grid functions in Ω^f . We define the three dimensional discrete scalar product in Ω^f similarly as in Ω^c

$$(\mathbf{u}, \mathbf{v})_h = h^3 \sum_{i=1}^{n^h} \sum_{j=1}^{n^h} \sum_{k=1}^{n^h} \omega_k J_{ijk}^h u_{ijk} v_{ijk},$$

and the two dimensional scalar product for grid functions on the interface Γ^f

$$\langle \mathbf{u}_{\Gamma^f}, \mathbf{v}_{\Gamma^f} \rangle_h = h^2 \sum_{i=1}^{n^h} \sum_{j=1}^{n^h} J_{\Gamma,ij}^h |\nabla^f r^3|_{ij} u_{ij} v_{ij}, \quad (24)$$

where J_{ijk}^h , u_{ijk} , v_{ijk} , $J_{\Gamma,ij}^h$, u_{ij} and v_{ij} have similar definitions as in (22) and (23).

Now, we are ready to present the energy conservation of the proposed schemes in Section 3.2. Multiplying (9) by $8h^3\omega_k \mathcal{J}^{2h} \mathbf{c}_t$ and summing over all grids, we have

$$(\mathbf{c}_t, \varrho^{2h} \mathbf{c}_{tt})_{2h} = (\mathbf{c}_t, \tilde{L}^{2h} \tilde{\mathbf{c}})_{2h} = -S_{2h}(\mathbf{c}_t, \mathbf{c}) + B_{2h}(\mathbf{c}_t, \tilde{\mathbf{c}}), \quad (25)$$

multiplying (16) by $h^3\omega_k \mathcal{J}^h \mathbf{f}_t$ and summing over all grids, we obtain

$$(\mathbf{f}_t, \varrho^h \mathbf{f}_{tt})_h = (\mathbf{f}_t, \hat{L}^h \mathbf{f})_h = -S_h(\mathbf{f}_t, \mathbf{f}) + B_h(\mathbf{f}_t, \mathbf{f}) + h^3\omega_1(\mathbf{f}_\Gamma)_t^T \boldsymbol{\eta},$$

where both S_{2h} and S_h are symmetric and positive definite bilinear forms, and

$$B_h(\mathbf{f}_t, \mathbf{f}) = -h^2(\mathbf{f}_\Gamma)_t^T (\mathcal{N}_{31}^h \mathcal{D}_1^h \mathbf{f}|_\Gamma + \mathcal{N}_{32}^h \mathcal{D}_2^h \mathbf{f}|_\Gamma + \mathcal{N}_{33}^h \mathcal{D}_3^h \mathbf{f}|_\Gamma), \quad (26)$$

and

$$B_{2h}(\mathbf{c}_t, \tilde{\mathbf{c}}) = 4h^2(\mathbf{c}_\Gamma)_t^T (\mathcal{N}_{31}^{2h} \mathcal{D}_1^{2h} \mathbf{c}|_\Gamma + \mathcal{N}_{32}^{2h} \mathcal{D}_2^{2h} \mathbf{c}|_\Gamma + \mathcal{N}_{33}^{2h} \tilde{\mathcal{D}}_3^{2h} \tilde{\mathbf{c}}|_\Gamma). \quad (27)$$

Then, the time derivative of the semi-discrete energy reads as

$$\begin{aligned} \frac{d}{dt} [(\mathbf{f}_t, \varrho^h \mathbf{f}_t)_h + S_h(\mathbf{f}, \mathbf{f}_t) + (\mathbf{c}_t, \varrho^{2h} \mathbf{c}_t)_{2h} + S_{2h}(\mathbf{c}, \mathbf{c}_t)] = \\ 2B_h(\mathbf{f}_t, \mathbf{f}) + 2B_{2h}(\mathbf{c}_t, \tilde{\mathbf{c}}) + 2h^3\omega_1(\mathbf{f}_\Gamma)_t^T \boldsymbol{\eta}, \end{aligned} \quad (28)$$

plugging (26)–(27) into (28) and combining the definition of the scalar product on the interface Γ (23)–(24), we have

$$\begin{aligned} & \frac{d}{dt} [(\mathbf{f}_t, \varrho^h \mathbf{f}_t)_h + S_h(\mathbf{f}, \mathbf{f}_t) + (\mathbf{c}_t, \varrho^{2h} \mathbf{c}_t)_{2h} + S_{2h}(\mathbf{c}, \mathbf{c}_t)] \\ &= 2 \left\langle (\mathbf{f}_\Gamma)_t, |\nabla^f r^3|^{-1} (\mathcal{J}_\Gamma^h)^{-1} (-\mathcal{A}_3^h \mathbf{f}|_\Gamma + h\omega_1 \boldsymbol{\eta}) \right\rangle_h + 2 \left\langle (\mathbf{c}_\Gamma)_t, |\nabla^c r^3|^{-1} (\mathcal{J}_\Gamma^{2h})^{-1} \tilde{\mathcal{A}}_3^{2h} \tilde{\mathbf{c}}|_\Gamma \right\rangle_{2h} \\ &= 2 \left\langle \tilde{\mathcal{P}}((\mathbf{c}_\Gamma)_t), |\nabla^f r^3|^{-1} (\mathcal{J}_\Gamma^h)^{-1} (-\mathcal{A}_3^h \mathbf{f}|_\Gamma + h\omega_1 \boldsymbol{\eta}) \right\rangle_h + 2 \left\langle (\mathbf{c}_\Gamma)_t, |\nabla^c r^3|^{-1} (\mathcal{J}_\Gamma^{2h})^{-1} \tilde{\mathcal{A}}_3^{2h} \tilde{\mathbf{c}}|_\Gamma \right\rangle_{2h} \\ &= 2 \left\langle (\mathbf{c}_\Gamma)_t, \tilde{\mathcal{R}}(|\nabla^f r^3|^{-1} (\mathcal{J}_\Gamma^h)^{-1} (-\mathcal{A}_3^h \mathbf{f}|_\Gamma + h\omega_1 \boldsymbol{\eta})) \right\rangle_{2h} + 2 \left\langle (\mathbf{c}_\Gamma)_t, |\nabla^c r^3|^{-1} (\mathcal{J}_\Gamma^{2h})^{-1} \tilde{\mathcal{A}}_3^{2h} \tilde{\mathbf{c}}|_\Gamma \right\rangle_{2h} = 0, \end{aligned}$$

where we have used the notaions in (20)–(21).

4 The temporal discretization

The equations are advanced in time with an explicit fourth order accurate predictor-corrector time integration method. Like all explicit time stepping methods, there is a maximum time step not exceed CFL stability limit.

In [3], it is proved that the time step constraint by CFL condition for the Newmark scheme

$$\varrho^h \frac{\mathbf{f}^{n+1} - 2\mathbf{f}^n + \mathbf{f}^{n-1}}{\Delta_t^2} = \hat{L}^h \mathbf{f}^n, \quad \varrho^{2h} \frac{\mathbf{c}^{n+1} - 2\mathbf{c}^n + \mathbf{c}^{n-1}}{\Delta_t^2} = \tilde{L}^{2h} \tilde{\mathbf{c}}^n, \quad n = 0, 1, \dots,$$

which is second order with

$$\frac{\Delta_t^2}{h^2} \kappa_{\max} \leq C_{\text{cfl}}^2$$

for the elastic wave equaiton with a homogeneous material and periodic boundary conditions. Here, κ_{\max} is the maximum of the eigenvalue of the matrices

$$T^{\{f,c\}} = \frac{1}{\rho^{\{f,c\}}} \begin{pmatrix} Tr(N_{11}^{\{f,c\}}) & Tr(N_{12}^{\{f,c\}}) & Tr(N_{13}^{\{f,c\}}) \\ Tr(N_{21}^{\{f,c\}}) & Tr(N_{22}^{\{f,c\}}) & Tr(N_{23}^{\{f,c\}}) \\ Tr(N_{31}^{\{f,c\}}) & Tr(N_{32}^{\{f,c\}}) & Tr(N_{33}^{\{f,c\}}) \end{pmatrix},$$

where $Tr(N_{ij}^{f,c})$ represents the trace of the matrix $N_{ij}^{f,c}, i, j = 1, 2, 3$. In this paper, we use the predictor-corrector strategy to obtain a fourth order time integrator. In [4], it shows that the fourth order scheme has a somewhat larger stability limit for the time step, but the way used to approximate eigenvalue is same. We use $C_{\text{cfl}} = 1.3175$ in the numrical experiments in this paper.

4.1 Time discretization with SBP scheme

In the following, we give the detailed procedures about how we apply the fourth order time integrator to the problems (9) and (16).

Let \mathbf{c}^n and \mathbf{f}^n denote the numerical approximations of $\mathbf{C}(\mathbf{x}, t_n), \mathbf{x} \in \Omega^c$ and $\mathbf{F}(\mathbf{x}, t_n), \mathbf{x} \in \Omega^f$ respectively. Here, $t_n = n\Delta_t, n = 0, 1, \dots$ and $\Delta_t > 0$ is a constant time step. We present the fourth order time integrator with predictor and corrector in the Algorithm 1.

Algorithm 1 Fourth order accurate time stepping for the elastic wave equation with SBP discretization in space

Given initial conditions $\tilde{\mathbf{c}}^0, \tilde{\mathbf{c}}^{-1}$ and $\mathbf{f}^0, \mathbf{f}^{-1}$ that satisfies the discretized interface conditions.

- Compute the predictor at the interior grid points for both fine and coarse domains

$$\mathbf{c}^{*,n+1} = 2\mathbf{c}^n - \mathbf{c}^{n-1} + \Delta_t^2 (\varrho^{2h})^{-1} \tilde{L}^{2h} \tilde{\mathbf{c}}^n, \quad \mathbf{f}^{*,n+1} = 2\mathbf{f}^n - \mathbf{f}^{n-1} + \Delta_t^2 (\varrho^h)^{-1} \hat{L}^h \mathbf{f}^n$$

- For the continuity of solution on the interface Γ , assign the value $\mathbf{f}_\Gamma^{*,n+1}$ to satisfy

$$\mathbf{f}_\Gamma^{*,n+1} = \tilde{\mathcal{P}}(\mathbf{c}_\Gamma^{*,n+1})$$

- For the continuity of traction on the interface Γ , assign the ghost points value in $\tilde{\mathbf{c}}^{*,n+1}$ to satisfy

$$|\nabla^c r^3|^{-1} (\mathcal{J}_\Gamma^{2h})^{-1} \tilde{\mathcal{A}}_3^{2h} \tilde{\mathbf{c}}^{*,n+1}|_\Gamma = \tilde{\mathcal{R}} \left(|\nabla^f r^3|^{-1} (\mathcal{J}_\Gamma^h)^{-1} (\mathcal{A}_3^h \mathbf{f}^{*,n+1}|_\Gamma - h\omega_1 \boldsymbol{\eta}^{*,n+1}) \right) \quad (29)$$

with the definition of $\tilde{\mathcal{A}}_3^{2h}$ in (21), \mathcal{A}_3^h in (20)

- Evaluate the acceleration at all grids

$$\tilde{\mathbf{c}}^n = \frac{\tilde{\mathbf{c}}^{*,n+1} - 2\tilde{\mathbf{c}}^n + \tilde{\mathbf{c}}^{n-1}}{\Delta_t^2}, \quad \mathbf{f}^n = \frac{\mathbf{f}^{*,n+1} - 2\mathbf{f}^n + \mathbf{f}^{n-1}}{\Delta_t^2}$$

- Compute the corrector at the interior grid points

$$\mathbf{c}^{n+1} = \mathbf{c}^{*,n+1} + \frac{\Delta_t^4}{12}(\varrho^{2h})^{-1}\tilde{\mathcal{L}}^{2h}\tilde{\mathbf{c}}^n, \quad \mathbf{f}^{n+1} = \mathbf{f}^{*,n+1} + \frac{\Delta_t^4}{12}(\varrho^h)^{-1}L^h\mathbf{f}^n$$

- For the continuity of solution on the interface Γ , assign the value \mathbf{f}_Γ^{n+1} to satisfy

$$\mathbf{f}_\Gamma^{n+1} = \tilde{\mathcal{P}}(\mathbf{c}_\Gamma^{n+1})$$

- For the continuity of traction on the interface Γ , assign the ghost point value in $\tilde{\mathbf{c}}^{n+1}$ to satisfy

$$|\nabla^c r^3|^{-1} (\mathcal{J}_\Gamma^{2h})^{-1} \tilde{\mathcal{A}}_3^{2h} \tilde{\mathbf{c}}^{n+1}|_\Gamma = \tilde{\mathcal{R}} \left(|\nabla^f r^3|^{-1} (\mathcal{J}_\Gamma^h)^{-1} (\mathcal{A}_3^h \mathbf{f}^{n+1}|_\Gamma - h\omega_1 \boldsymbol{\eta}^{n+1}) \right) \quad (30)$$

with the definition of $\tilde{\mathcal{A}}_3^{2h}$ in (21), \mathcal{A}_3^h in (20)

Here, we only give the steps to evolve the elatic wave equation with suitable initial and interface conditions and skip the detailed derivations of the fourth order predictor corrector time integrator. One can refer to [6] to get more details.

In the Algorithm 1, we need to solve the equations come from the continuity of the traction force for the interface Γ in both preditor step (29) and corrector step (30). The structure of (29) and (30) are same, for simplicity, we only clarify how we solve (29) in the predictor step.

Note that there are $3n^{2h}n^{2h}$ unknowns in (29) and $3n^{2h}n^{2h}$ linear equations in (29). Since it is very expensive to calculate the LU-factorization for a large problem in 3D and there is no efficient ways to calculate the LU-factorization in a parallel machine, we instead using iterative methods to solve the linear system (29). Specifically, we use three different iterative methods: block Jacobian iterative method, conjugate gradient iterative method, pre-conditioned conjugate gradient iterative method, to solve (29). The details are given in Section 5.1.1.

5 Numerical Experiments

In this section, we conduct several numerical experiments. In Section 5.1, we compare the efficiency of iterative methods which are used to solve the interface condition system (29) and (30), note that the coefficient matrices in (29) and (30) are same, verify the order of the convergence of the proposed scheme (9), (16) and (18)–(19). In Section 5.2, we show that there is no reflection at the mesh refinement interfaces for the proposed scheme (9), (16) and (18)–(19) with only a traction force on the top surface. Finally, the energy conservation property is shown in Section 5.3.

5.1 Method of manufactured solutions

We take the computation domain to be

$$\begin{cases} x^{c,(1)} = 2\pi r^{(1)} \\ x^{c,(2)} = 2\pi r^{(2)} \\ x^{c,(3)} = r^{(3)}\theta_i(r^{(1)}, r^{(2)}) + (1 - r^{(3)})\theta_b(r^{(1)}, r^{(2)}) \end{cases} \quad (31)$$

for coarse domain Ω_c . Here, $0 \leq r^{(1)}, r^{(2)}, r^{(3)} \leq 1$, f_i is the interface surface geometry,

$$\theta_i(r^{(1)}, r^{(2)}) = \pi + 0.2 \sin(4\pi r^{(1)}) + 0.2 \cos(4\pi r^{(2)}), \quad (32)$$

and θ_b is the bottom surface geometry,

$$\theta_b(r^{(1)}, r^{(2)}) = 0.2 \exp\left(-\frac{(r^{(1)} - 0.6)^2}{0.04}\right) + 0.2 \exp\left(-\frac{(r^{(2)} - 0.6)^2}{0.04}\right). \quad (33)$$

As for the fine domain Ω_f , it is chosen to be

$$\begin{cases} x^{f,(1)} = 2\pi r^{(1)} \\ x^{f,(2)} = 2\pi r^{(2)} \\ x^{f,(3)} = r^{(3)}\theta_t(r^{(1)}, r^{(2)}) + (1 - r^{(3)})\theta_i(r^{(1)}, r^{(2)}), \end{cases} \quad (34)$$

where $0 \leq r^{(1)}, r^{(2)}, r^{(3)} \leq 1$, θ_t is the top surface geometry,

$$\theta_t(r^{(1)}, r^{(2)}) = 0.2 \exp\left(-\frac{(r^{(1)} - 0.5)^2}{0.04}\right) + 0.2 \exp\left(-\frac{(r^{(2)} - 0.5)^2}{0.04}\right), \quad (35)$$

and θ_i is the interface geometry which is given in (32). Note that the subdomain Ω_f is on the top of the subdomain Ω_c . For both fine and coarse domains, let the density vary according to

$$\rho(x^{(1)}, x^{(2)}, x^{(3)}) = 2 + \sin(x^{(1)} + 0.3) \sin(x^{(2)} + 0.3) \sin(x^{(3)} - 0.2), \quad (36)$$

and material parameters μ, λ satisfy

$$\mu(x^{(1)}, x^{(2)}, x^{(3)}) = 3 + \sin(3x^{(1)} + 0.1) \sin(3x^{(2)} + 0.1) \sin(x^{(3)}), \quad (37)$$

and

$$\lambda(x^{(1)}, x^{(2)}, x^{(3)}) = 21 + \cos(x^{(1)} + 0.1) \cos(x^{(2)} + 0.1) \sin^2(3x^{(3)}), \quad (38)$$

respectively. Besides, we impose a boundary forcing on the top surface and Dirichlet boundary conditions for the other boundaries. The internal forcing \mathbf{F} , top boundary forcing \mathbf{g} and initial conditions are chosen such that $\mathbf{u} = (u_1, u_2, u_3)^T$ with

$$\begin{aligned} u_1 &= \cos(x^{(1)} + 0.3) \sin(x^{(2)} + 0.3) \sin(x^{(3)} + 0.2) \cos(t^2), \\ u_2 &= \sin(x^{(1)} + 0.3) \cos(x^{(2)} + 0.3) \sin(x^{(3)} + 0.2) \cos(t^2), \\ u_3 &= \sin(x^{(1)} + 0.2) \sin(x^{(2)} + 0.2) \cos(x^{(3)} + 0.2) \sin(t). \end{aligned}$$

For example, for the boundary forcing on the top surface, we impose

$$\mathbf{g} = (g_1, g_2, g_3)^T = \sum_{i=1}^3 \left(\sum_{j=1}^3 M_{ij}^f \frac{\partial \mathbf{u}}{\partial x^{(j)}} \right) n^{(i)}, \quad (39)$$

where, $n^{(i)}$ is the element of the unit outward normal $\mathbf{n} = (n^{(1)}, n^{(2)}, n^{(3)})$ for the top surface.

5.1.1 Iterative methods

In the proposed scheme (9), (16) and (18)–(19), we need to solve a $3n^{2h}n^{2h} \times 3n^{2h}n^{2h}$ linear system at each time step twice for the continuity of the traction force along the interface (29) and (30). Even though we can do LU factorization one time before the time loop start and reuse it at each time step, it is very expensive to do LU factorization for a large problem. Besides, consider solving real problems which are usually in large scale, we want to perform the computation on many processors on a parallel distributed memory machine, but it is not clear how to calculate the LU factorization of a matrix on many processors.

In this paper, we propose three iterative methods: block Jacobian method, conjugate gradient method, preconditioned conjugate gradient method. We find that preconditioned conjugate gradient method is the most efficient one and conjugate gradient method needs most iteration numbers.

For the problem proposed in Section 5.1, the structure of the coefficient matrix of the linear system (19) is shown in Figure 5 which is determined by the interpolation operator $\tilde{\mathcal{P}}$ and restriction operator $\tilde{\mathcal{R}}$. We choose the red circles in the purple circles in Figure 5 to be the block Jacobian matrix in block Jacobian iterative method and pre-conditioning matrix in pre-conditioned conjugate gradient iterative method. We also set a absolute error tolerance $1e - 7$ for each iterative method.

$h_k^c = 2h_k^f$	CG	Block Jacobian	Preconditioned CG
$2\pi/24$	37.78	24.96	4.01
$2\pi/48$	38.61	25.38	2.87
$2\pi/96$	39.14	25.43	2.55

Table 1: condition number of matrices in conjugate gradient method, block Jacobian method, preconditioned conjugate gradient method

Table 1 shows the condition number of the original coefficient matrix, the block Jacobian matrix and the coefficient matrix after applying pre-conditioner respectively. We observe that the condition number for preconditioned conjugate gradient method is smallest which is consistent with the results for iteration number of different iterative methods : there is around 44 iterations for conjugate gradient method, 13 iterations for block Jacobian method and 9 iterations for preconditioned conjugate method.

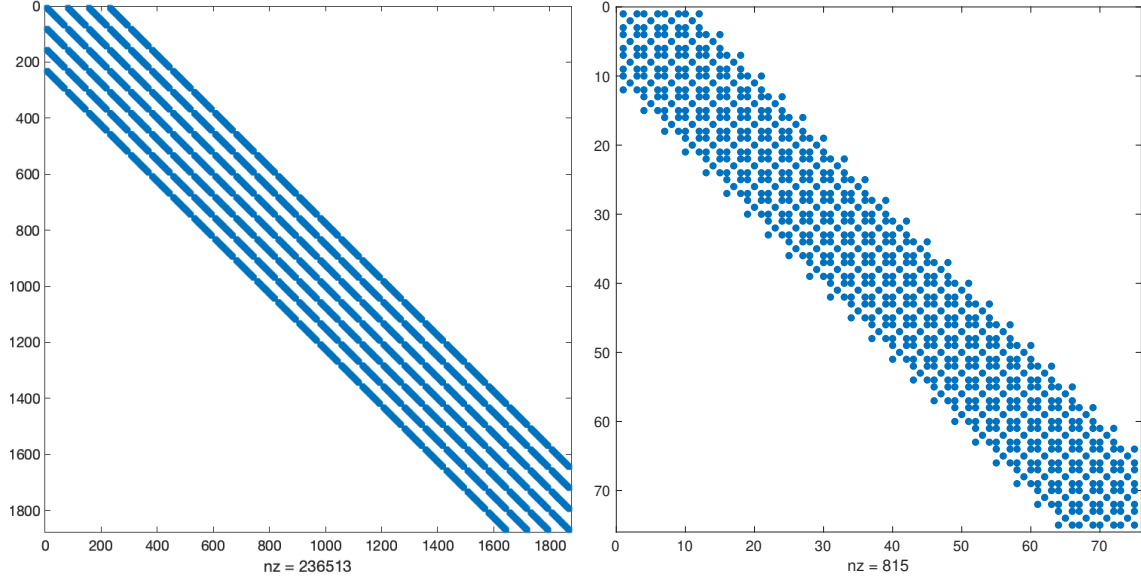


Figure 5: The left panel is the structure of the coefficient matrix of the linear system (19). The right panel is the zoom in structure for the repeated pattern on the left panel.

5.1.2 Verification of convergence rate

We now perform a convergence study for the proposed scheme (9), (16) and (18)–(19). The convergence rate is computed by

$$\log \left(\frac{e_h}{e_{2h}} \right) / \log \left(\frac{1}{2} \right),$$

here, e_h is the corresponding L^2 error. The problem is evolved until final time $T = 0.5$. The L^2 error for the numerical solutions in the whole domain, $L^{f,2}$ error for the numerical solutions in the fine domain Ω^f and $L^{c,2}$ error for the numerical solutions in the coarse domain Ω^c are presented in Table 2. We observe that the convergence rate is fourth order for all cases, thought the theoretical convergence rate is second for the points near boundaries. Note that we use a block Jacobian iterative method for the experiments here.

$h^c = 2h^f$	L^2	$L^{f,2}$	$L^{c,2}$
$2\pi/24$	2.2227e-03	8.0442e-04	2.0720e-03
$2\pi/48$	1.4142e-04 (3.97)	5.1478e-05 (3.97)	1.3171e-04 (3.98)
$2\pi/96$	8.6166e-06 (4.04)	3.0380e-06 (4.08)	8.0632e-06 (4.03)

Table 2: Convergence rate of the fourth order SBP method

5.2 Gaussian source

In this section, we present the numerical experiments to illustrate that there is no obvious artifacts are generated by the curvilinear interface. Specifically, we test the problem on the computation

domain

$$\begin{cases} x^{c,(1)} = 2000r^{(1)} \\ x^{c,(2)} = 2000r^{(2)} \\ x^{c,(3)} = r^{(3)}\theta_i(r^{(1)}, r^{(2)}) + (1 - r^{(3)})\theta_b(r^{(1)}, r^{(2)}) \end{cases} \quad (40)$$

for coarse domain Ω_c . Here, $0 \leq r^{(1)}, r^{(2)}, r^{(3)} \leq 1$, θ_i is the interface surface geometry,

$$\theta_i(r^{(1)}, r^{(2)}) = 800 + 20 \sin(4\pi r^{(1)}) + 20 \cos(4\pi r^{(2)}), \quad (41)$$

and θ_b is the bottom surface geometry,

$$\theta_b(r^{(1)}, r^{(2)}) = 0. \quad (42)$$

As for the fine domian Ω_f , it is choose to be

$$\begin{cases} x^{f,(1)} = 2000r^{(1)} \\ x^{f,(2)} = 2000r^{(2)} \\ x^{f,(3)} = r^{(3)}\theta_t(r^{(1)}, r^{(2)}) + (1 - r^{(3)})\theta_i(r^{(1)}, r^{(2)}), \end{cases} \quad (43)$$

where $0 \leq r^{(1)}, r^{(2)}, r^{(3)} \leq 1$, θ_t is the top surface geometry,

$$\theta_t(r^{(1)}, r^{(2)}) = 1000, \quad (44)$$

and θ_i is the interface geometry which is given in (32). Note that the subdomian Ω_f is on the top of Ω_c . For both fine and coarse domians, let the density vary according to

$$\rho(x^{(1)}, x^{(2)}, x^{(3)}) = 1.5 \times 10^3, \quad (45)$$

and material parameters μ, λ satisfy

$$\mu(x^{(1)}, x^{(2)}, x^{(3)}) = 1.5 \times 10^9, \quad \lambda(x^{(1)}, x^{(2)}, x^{(3)}) = 3 \times 10^9, \quad (46)$$

respectively. Besides, we impose a Gaussian source on the top surface

$$\mathbf{g} = (g_1, g_2, g_3)^T,$$

where, $g_1 = g_2 = 0$, and

$$g_3 = 10^9 \exp \left(- \left(\frac{t - 4/44.2}{1/44.2} \right)^2 \right) \exp \left(- \left(\frac{x^{(1)} - 1000}{12.5} \right)^2 - \left(\frac{x^{(2)} - 1000}{12.5} \right)^2 \right).$$

Homogenerous Dirichlet boundary conditions are imposed to the other boundaries. The internal forcing \mathbf{F} is choosen to be zeros everywhere and the initial condition is also setted to be zero everywhere, $\mathbf{u} = \mathbf{0}$ at $t = 0$.

To compare the results, we use the solutions from a flat interface surface, $\theta_i(r^{(1)}, r^{(2)}) = 0$, with only Cartesian grids and no mesh refinement. Specifically, denote (n_1^c, n_2^c, n_3^c) to be the number of grid points in the coarse domian Ω_c , (n_1^f, n_2^f, n_3^f) to be the number of grid points in the fine domian Ω_f , (n_1, n_2, n_3) to be the number of grid points for the reference solution.

In the simulation of the reference solution, we choose $n_1 = n_2 = 201, n_3 = 101$. And in the experiments for the curvilinear interface with mesh refinement, we have $n_1^c = n_2^c = 101, n_3^c = 41$ and $n_1^f = n_2^f = 201, n_3^f = 21$. The numerical simulations are conducted until $T = 0.4$.

From Figure 6, Figure 7 and Figure 8, we observe that there is no significant reflection at the mesh refinement interfaces.

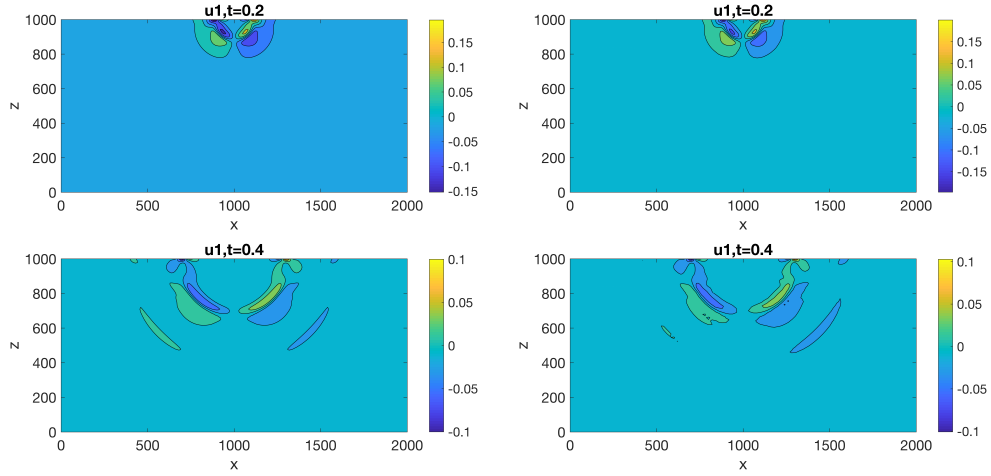


Figure 6: The graph for u_1 . From left to right are for Cartesian mesh without mesh refinement and curvi-linear mesh with mesh refinement respectively. From top to bottom are for $t = 0.2$ and $t = 0.4$ respectively.

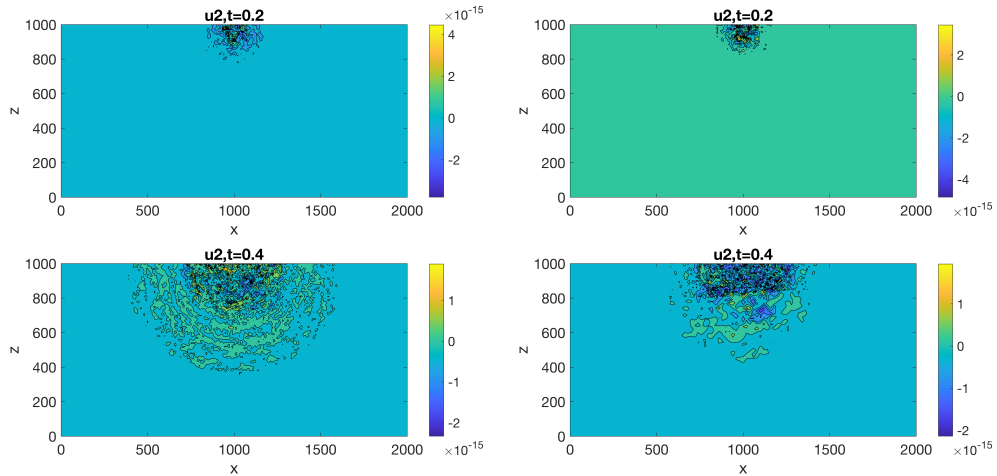


Figure 7: The graph for u_2 . From left to right are for Cartesian mesh without mesh refinement and curvi-linear mesh with mesh refinement respectively. From top to bottom are for $t = 0.2$ and $t = 0.4$ respectively.

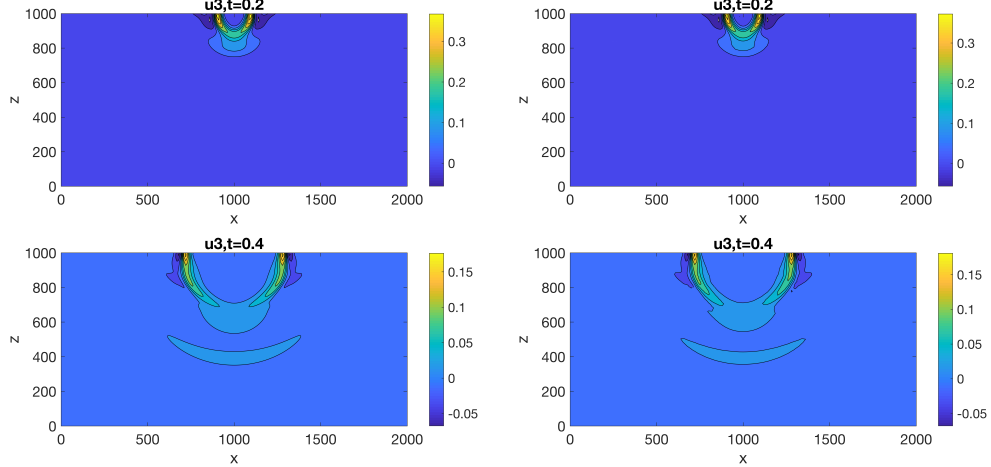


Figure 8: The graph for u_3 . From left to right are for Cartesian mesh without mesh refinement and curvi-linear mesh with mesh refinement respectively. From top to bottom are for $t = 0.2$ and $t = 0.4$ respectively.

5.3 Energy conservation test

We shall have an experiment for energy conservation. We also need to evaluate the iterative methods. These can be Experiment 3, or incorporated in the first two experiments.

6 Conclusion

A Appendix

$$P_1^T = \begin{pmatrix} 1 & 0 & 0 & 0 & 0 & 0 \\ 0 & 0 & 0 & 0 & 0 & 1 \\ 0 & 0 & 0 & 0 & 1 & 0 \end{pmatrix}, P_2^T = \begin{pmatrix} 0 & 0 & 0 & 0 & 0 & 1 \\ 0 & 1 & 0 & 0 & 0 & 0 \\ 0 & 0 & 0 & 1 & 0 & 0 \end{pmatrix}, P_3^T = \begin{pmatrix} 0 & 0 & 0 & 0 & 1 & 0 \\ 0 & 0 & 0 & 1 & 0 & 0 \\ 0 & 0 & 1 & 0 & 0 & 0 \end{pmatrix},$$

References

- [1] Kenneth Duru and Kristoffer Virta. Stable and high order accurate difference methods for the elastic wave equation in discontinuous media. *Journal of Computational Physics*, 279:37–62, 2014.
- [2] Ken Mattsson and Jan Nordström. Summation by parts operators for finite difference approximations of second derivatives. *Journal of Computational Physics*, 199(2):503–540, 2004.
- [3] N Anders Petersson and Björn Sjögreen. Wave propagation in anisotropic elastic materials and curvilinear coordinates using a summation-by-parts finite difference method. *Journal of Computational Physics*, 299:820–841, 2015.
- [4] Björn Sjögreen and N Anders Petersson. A fourth order accurate finite difference scheme for the elastic wave equation in second order formulation. *Journal of Scientific Computing*, 52(1):17–48, 2012.

- [5] Joe F Thompson, Zahir UA Warsi, and C Wayne Mastin. Numerical grid generation: foundations and applications, volume 45. North-holland Amsterdam, 1985.
- [6] Siyang Wang and N Anders Petersson. Fourth order finite difference methods for the wave equation with mesh refinement interfaces. arXiv preprint arXiv:1809.04310, 2018.